applied optics

Analysis of plasmonic phase modulator with furan–thiophene chromatophore electro-optic polymer

Naoya Hojo,[1] Tomohiro Amemiya,[1,2,*] Kazuto Itoh,[1] Zhichen Gu,[1] Chiyumi Yamada,[3] Toshiki Yamada,[3] Junichi Suzuki,[1] Yusuke Hayashi,[1] Nobuhiko Nishiyama,[1,2] Akira Otomo,[3] and Shigehisa Arai[1,2]

[1]Department of Electrical and Electronic Engineering, Tokyo Institute of Technology, Meguro-ku, Tokyo 152-8552, Japan
[2]Institute of Innovative Research (IIR), Tokyo Institute of Technology, Meguro-ku, Tokyo 152-8552, Japan
[3]National Institute of Information and Communications Technology, Kobe-shi, Hyogo 651-2492, Japan
*Corresponding author: amemiya.t.ab@m.titech.ac.jp

Received 28 December 2016; revised 8 February 2017; accepted 8 February 2017; posted 8 February 2017 (Doc. ID 283399); published 3 March 2017

We analyzed two types of Mach–Zehnder plasmonic modulators on a silicon-on-insulator platform with a different furan–thiophene chromophore electro-optic polymer to compare to other reports. The metal-taper coupling structure and the metal-insulator-metal cross section in our design have been optimized based on the new material parameters. According to the simulation result, a modulator with a slot width of 50 nm and an on–off voltage of $V\pi = 20$ V can be 21 μm long, leading to a total modulator loss of 15 dB, which is comparable to previously reported devices. © 2017 Optical Society of America

OCIS codes: (250.2080) Polymer active devices; (250.5403) Plasmonics; (130.4110) Modulators.

https://doi.org/10.1364/AO.56.002053

1. INTRODUCTION

In accordance with the expected Internet traffic explosion in the future, photonic integrated circuits (PICs) play an increasing role in information systems owing to their potential in boosting the data transmission speed at lower power and cost. InP-based passive optical components, such as modulators, switches, or photodetectors, are well known to be commonly used in PICs considering their integration with III–V compound laser sources [1,2]. As a next-generation technology, Si photonics has been proven to be a promising solution for lower-cost and higher-performance PICs in recent years to possibly provide low loss and high-density integration, in addition to their compatibility with the complementary metal–oxide–semiconductor (CMOS) process [3,4]. Although InP still maintains the lead role in the race for material dominant in optical components, worldwide researchers have become increasingly interested in the revolution of PICs based on other types of materials.

In the past few years, surface plasmon polariton (SPP), which involves both the charge motion in metals and electromagnetic waves in air or a dielectric, has come into prominence among all the research fields toward the realization of further downscaled high-performance PICs [5,6]. This type of surface waveguide along the interface between the metal and dielectric can be expected to provide subwavelength-scale optical confinement [7–9], hence making great contribution to the performance development of key components in PICs, such as a low-power-consumption laser source [10–13], high-density integration of downscaled optical waveguides [14–16], or high-speed photodetector with ultra-small capacitance [17–20], among others.

Similar to the abovementioned components, miniaturization of optical modulators (~10 μm) can also be achieved by utilizing the SPP phenomenon that could provide extremely strong optical confinement. Recently, the electro-absorption modulation realized by controlling the carrier concentration of a transparent conductive material layer such as indium–tin–oxide [21–23] and the electro-optic (EO) phase modulation based on the refractive index variation of the EO polymer [24–28] have been considered as the two most promising solutions to the mechanism of the so-called plasmonic modulator. Both processes have been vigorously studied worldwide, whereas the propagation loss caused by metal absorption in these two designs still tends to be the biggest barrier in the practical use, which far outweighs the advantage of providing smaller value of voltage-length product ($V_\pi L$) (i.e., larger extinction ratio with the same device length and the same applied voltage) than the conventional optical modulators.

Here, we considered two approaches for plasmonic modulators, namely, silicon-plasmonic [27] and all-plasmonic [29] approaches (some simulative investigations and experimental results of these two approaches can be found in [30] for the

silicon-plasmonic one and in [31] for the all-plasmonic one). In this paper, through detailed electromagnetic analysis, we investigated these approaches for a plasmonic modulator with a metal-taper structure embedded by a furan–thiophene chromophore EO polymer (FTC-EO polymer).

2. MODULATOR CONCEPT

In plasmonic modulators, optical modulation is normally realized by controlling the properties of certain types of functional materials where ultra-high-intensity light is confined based on the SPP effect. Therefore, effective excitations of SPPs in a well-designed waveguide structure and larger change in the optical properties of the functional materials have become the two most important factors in the current study.

In this work, we analyze two types of plasmonic push–pull modulators, i.e., a partial plasmonic modulator [Fig. 1(a)] and a whole plasmonic modulator [Fig. 1(b)], which can be monolithically integrated with conventional Si photonic waveguides. They both consist of Mach–Zehnder (MZ) interferometers with metal–insulator–metal (MIM) slot waveguides embedded by a specific EO polymer.

The partial plasmonic modulator introduces the MIM slot waveguide only in the phase-shifting region of the device [20]. This type, which was first demonstrated by Melikyan *et al.* [27], is quite simple and more reliable to fabricate. A more advanced experiment demonstrated the applicability in compact transmitters for optical interconnect [32,33].

On the other hand, the whole plasmonic modulator proposed by Zhu *et al.* [34] uses the MIM slot waveguide to construct an entire MZ interferometer, including a 1×2 splitter and combiner. This type has also been demonstrated applicability in more complex optical integrated circuits, such as the IQ modulator [29,31].

Although the above results are highly valuable, they are still in the experimental stage and suffer from various problems. Typically, shorter devices allow for smaller insertion loss; however, extinction ratio per driving voltage becomes smaller at the same time. On the contrary, longer devices allow for higher extinction ratio per voltage; however, this comes at the price of insertion loss. Therefore, striking a balance between high extinction ratio and low transmission loss must always be considered.

In the devices shown in Fig. 1, the abovementioned problems can be solved by considering the following two points:

(i) A metal-taper structure [35,36] is introduced to enhance coupling efficiency between the Si and plasmonic waveguides. In this work, we optimized the taper structure for the materials used in the device.

(ii) An EO polymer with higher EO coefficient and higher voltage endurance is desirable to shorten devices (that is, reduce insertion loss) maintaining extinction ratio. Here, we assumed to use the FTC-EO polymer with improved optical properties for the long π-conjugated nonlinear optical chromophores having an amino-benzene donor with methoxy or benzyloxy groups [37,38]. Such a material type can provide good performance balance with a relatively large EO coefficient (75 pm/V), appropriate voltage endurance, and excellent thermal stability.

In the following sections, the feasibility of employing Si-based plasmonic modulators combined with the FTC-EO polymer is examined theoretically. In Section 3, we present the mode analysis of an MZ arm region consisting of an MIM waveguide embedded by the FTC-EO polymer. In Section 4, the transmission characteristics of entire devices, including the coupling regions between the Si and MIM waveguides, are then confirmed with the aid of computer simulation based on the finite-difference time-domain (FDTD) method. The simulation shows that the off-state insertion losses of the partial and whole plasmonic modulators are 13.7 and 15 dB with total device lengths of 19.3 and 21 μm, respectively, which features both small insertion loss and short device size compared to the

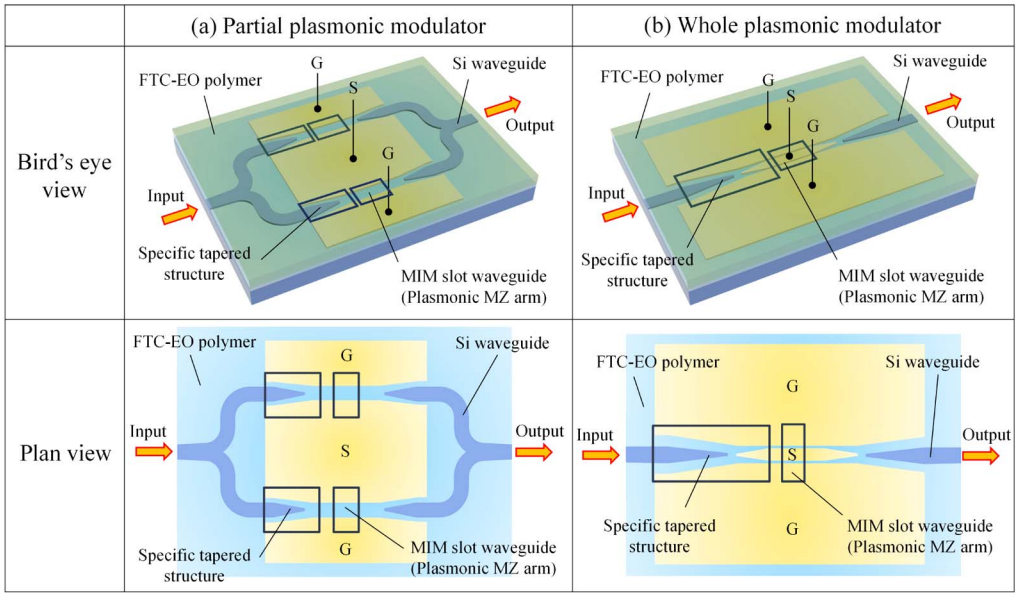

Fig. 1. Schematic of two types of plasmonic push–pull modulators. (a) Partial plasmonic modulator that introduces the MIM slot waveguide only in a phase-shifting region of the device. (b) Whole plasmonic modulator that uses the MIM slot waveguide to construct an entire MZ interferometer.

conventional plasmonic modulators [28–30]. Finally, Section 5 concludes this paper.

3. MODE ANALYSIS AND MODULATION CHARACTERISTIC OF THE MIM SLOT WAVEGUIDE

We first optimized the cross-sectional structure of the MIM waveguide used for the MZ arms in both devices shown in Fig. 1. Figure 2(a) shows a cross section of the device. In this structure, the gap-SPP (GSPP) waves are excited inside a metal slot, which produces strong optical confinement in the waveguide beyond the limit of diffraction, as shown in Fig. 2(b). The confined mode field induced by the GSPPs is substantially covered by the cross section of the FTC-EO polymer. Therefore, the light transmission can be effectively modulated when the optical properties of the FTC-EO polymer are varied by applying an external voltage.

To discuss the performance of a plasmonic modulator with a large metal absorption, we introduce two important figures of merit (FOMs). One is $V_\pi L(\mathrm{V}\cdot\mathrm{cm})$, which is a commonly used parameter for performance evaluation of phase modulators. The other is the propagation loss per unit length of the MIM slot waveguide. Applied voltage together with the $V_\pi L$ product determines the device length and therefore the insertion loss of the modulator.

We simulated $V_\pi L$ and the propagation loss per unit length of the MIM slot waveguide. To achieve this, we first calculated lines of electric force around the device when applying a specific driving voltage, using COMSOL Multiphysics simulation software. From the calculated lines of electric force and an EO coefficient of the FTC-EO polymer, we determined the profile of the optical constant around the MIM slot waveguide. We then calculated the distribution of the SPP waves in the device, using the finite element method with a perfectly matched layer boundary condition. $V_\pi L$ and propagation loss per unit length can be obtained from the complex refractive index of the MIM slot waveguide for each SPP wave state.

In the above simulation, we varied slot width W_{slot} from 50 to 500 nm. The refractive indices of Si, SiO_2, and FTC were set to 3.45, 1.45, and 1.529, respectively. In addition, the complex refractive index of the gold was assumed to be 0.469-9.32i. The EO constant of the FTC was set to 75 pm/V. Metal thickness h was designed to be 220 nm by considering the mode coupling efficiency between the MIM slot waveguide and the 220-nm-high Si input/output waveguide.

Figure 2(c) shows the calculated $V_\pi L$ and propagation loss per unit length w/o applied voltage of the MIM slot waveguide as a function of the slot width. We can see that smaller $V_\pi L$ can be obtained with narrower W_{slot} because the mode confinement is enhanced by stronger gap plasmon effect, which leads to a lower required external voltage. However, the propagation

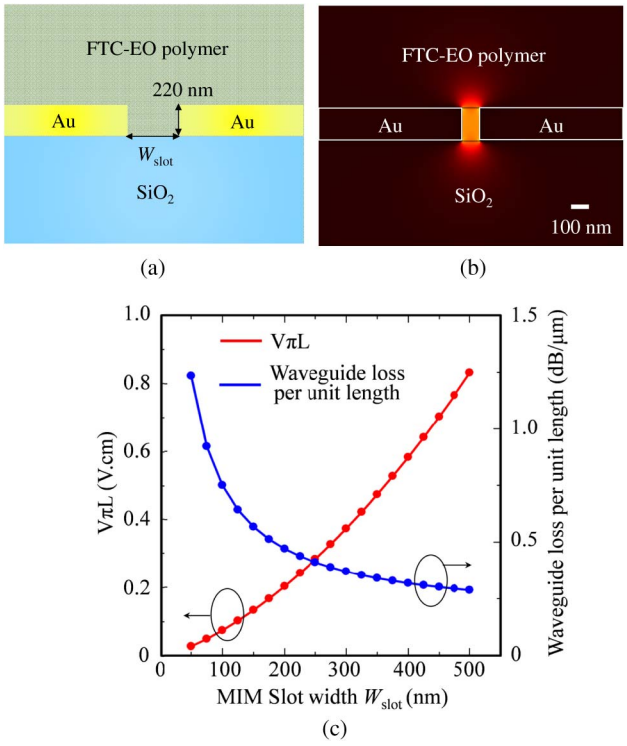

Fig. 2. (a) Cross-sectional view of the MIM slot waveguide. (b) Calculated mode distribution profile in a 100-nm MIM slot waveguide. (c) Calculated $V_\pi L$ and the propagation loss per unit length w/o applied voltage of the MIM slot waveguide with different slot widths.

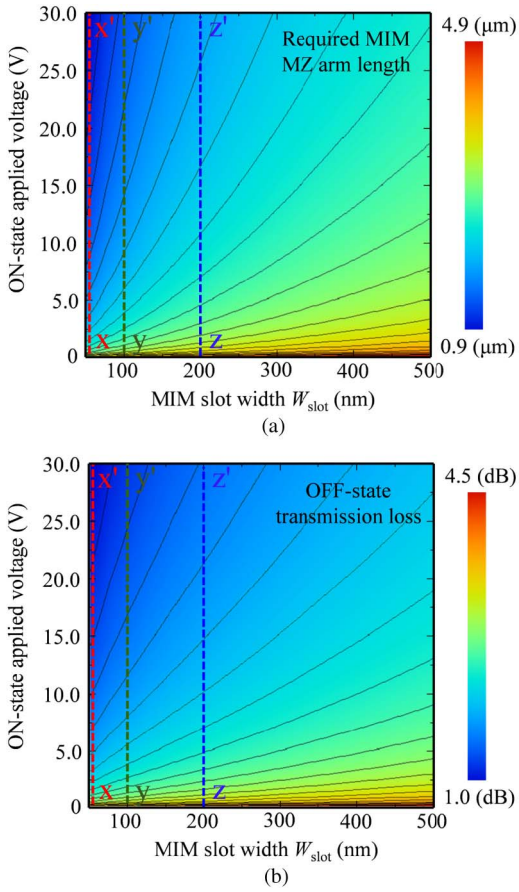

Fig. 3. (a) Required MZ arm length to obtain a $\pi/2$ phase shift with different applied voltages and plasmon slot widths. (b) Corresponding insertion loss.

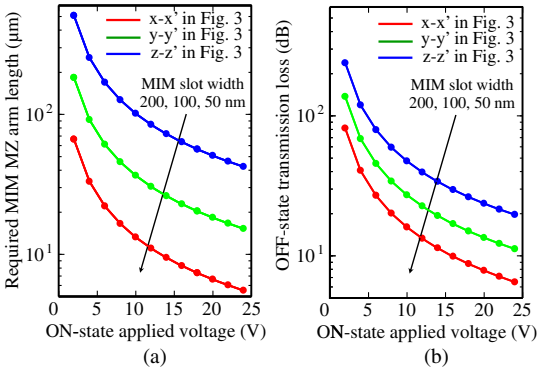

Fig. 4. (a) Required MZ arm length to obtain a $\pi/2$ phase shift and (b) insertion loss as a function of the applied voltage. The red, green, and blue lines correspond to x-x', y-y', and z-z' lines in Fig. 3, respectively.

loss per unit length would also drastically increase due to the intense excitation of the GSPP mode in a waveguide with a narrower slot.

Figure 3 shows (a) the required MZ arm length to obtain $\pi/2$ phase shift and (b) the insertion loss as a function of slot width W_{slot} and the external applied voltage. Clearly, a larger electric field inside the slot will provide a stronger EO effect in the FTC-EO polymer, which reduces the required MZ arm length and the related propagation loss.

Figure 4 shows the required MZ arm length and the insertion loss as a function of the applied voltage. The red, green, and blue lines shown in Fig. 4 correspond to the x-x', y-y', and z-z' lines shown in Fig. 3, respectively. For conclusion, we considered an arm length of 6.5 μm with a metal slot width of 50 nm as an appropriate structure, which is capable of providing $\pi/2$ phase modulation with an 8.1-dB propagation loss under an applied voltage of 20 V (20 V applied to a 50 nm slot waveguide is the withstand voltage limit for the FTC-EO polymer). Comparing our results with those reported in [28–30], the insertion loss in our design is relatively small, and our results present comparable modulation characteristics.

On the basis of the above discussion, in the next sections, we present the setting of metal slot width W_{slot} and thickness h of the MIM waveguide to 220 and 50 nm, respectively.

4. MODE COUPLING BETWEEN THE SI AND PLASMON WAVEGUIDES

In addition to the cross-sectional design of the MIM waveguide, the coupling efficiency between the input/output Si waveguides and the MIM waveguide is also an important element. Therefore, we calculated the transmission characteristic between the Si and MIM waveguides using the FDTD method. In the following, a detailed analysis of each device, namely, the partial and the whole plasmonic modulators, is described.

A. Partial Plasmonic Modulator

Figure 5(a) shows a plan view of the coupling region between the Si and plasmon waveguides in a partial plasmonic modulator. A metal-taper structure is introduced to enhance the coupling efficiency between the Si and MIM slot waveguides.

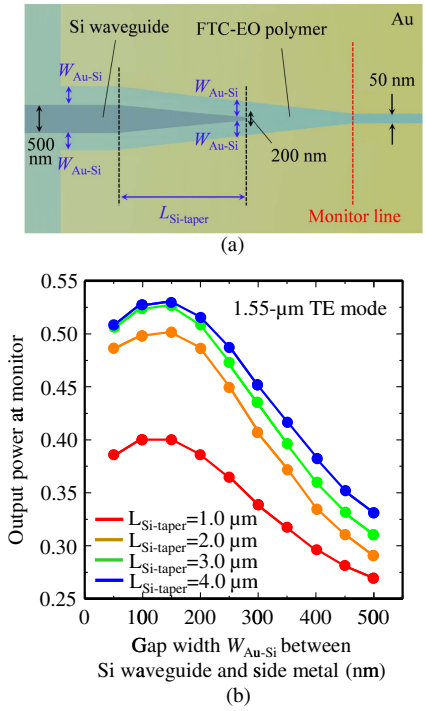

Fig. 5. (a) Schematic plan view of a coupling region between Si and plasmon waveguides in a partial plasmonic modulator. (b) Calculated conversion efficiency into SPPs initiated by tapering down a silicon waveguide, with the gap width and the Si taper length as parameters.

In this structure, the conversion into SPPs is initiated by tapering down the Si waveguide and transferring the plasmonic modes onto the MIM waveguide.

We calculated the conversion efficiency of the SPPs initiated by tapering down the Si waveguide. Here, the width and thickness of the input/output Si waveguides were fixed at 500 and 220 nm, respectively. The metal slot width and thickness of the MIM waveguide were also set to 220 and 50 nm based on the simulation results presented in Section 3. In this simulation, we varied two dimension parameters, namely, $L_{\text{Si-taper}}$ and $W_{\text{Au-Si}}$. Here, $L_{\text{Si-taper}}$ and $W_{\text{Au-Si}}$ are the length of the tapered Si waveguide and the gap width between the tapered Si waveguide and a side metal, respectively. Figure 5(b) shows the calculated power ratio at the inlet of the MIM waveguide [denoted as the monitor line in Fig. 5(a)]. With the decrease in gap width $W_{\text{Au-Si}}$, the distribution profile of the light started to be drawn toward both sides of the metal, which led to an efficient conversion into SPPs. In addition, a shorter taper length (or a steeper inclination angle) would make the propagation mode unstable and scatter into the cladding layer, which will also reduce the coupling efficiency to some extent. For the same reason, we also chose a flat end of the Si waveguide instead of tapering it down to a tip. As a result, appropriate coupling efficiency of 2.8 dB was obtained when $W_{\text{Au-Si}}$ and $L_{\text{Si-taper}}$ were set to 150 and 2.5 μm, respectively. It should be noticed that the loss induced by the Y splitter/combiner has also been taken into account in the coupling loss, which is less than 1 dB according to the calculation result based on the finite-difference method.

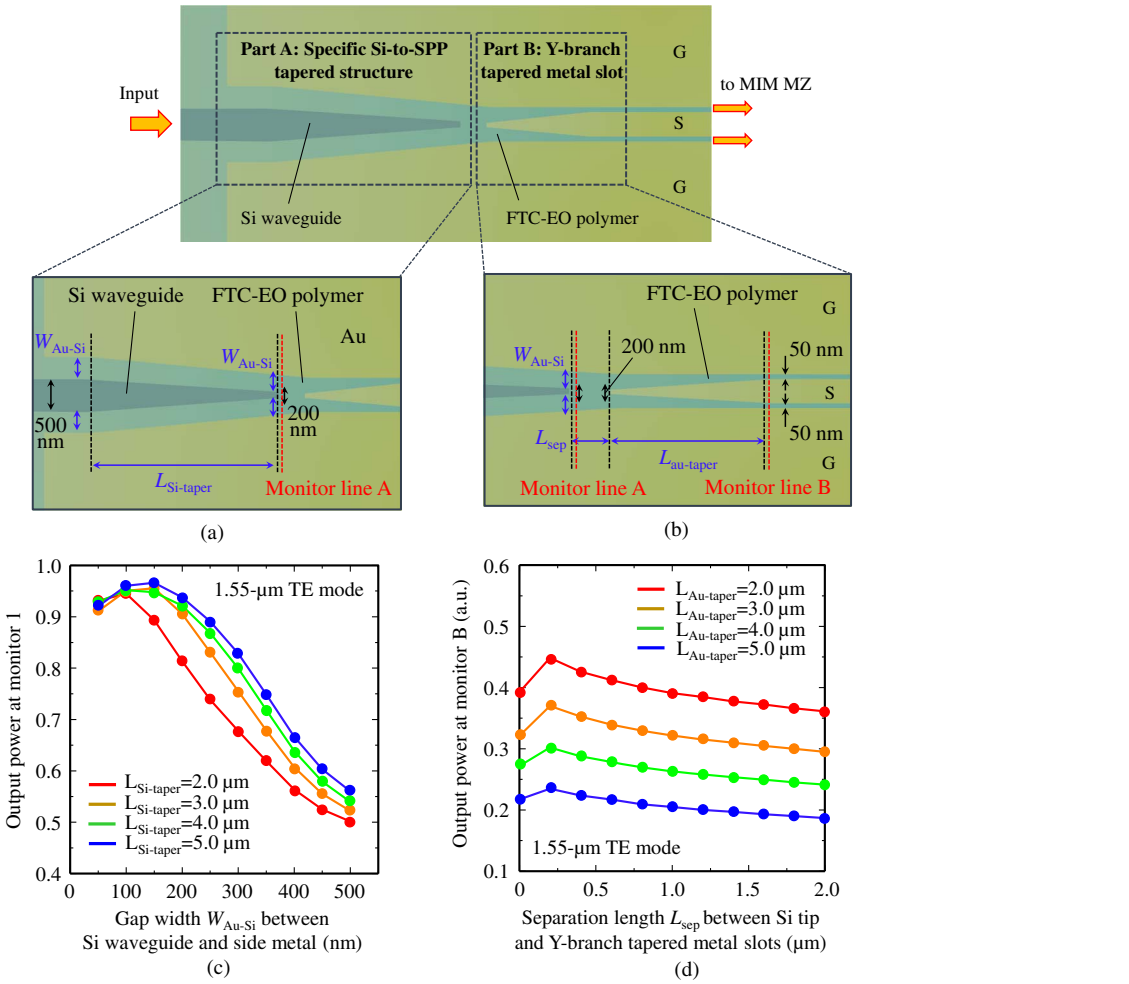

Fig. 6. (a) Schematic plan view of the first part of a coupling region between Si and plasmon waveguides in a whole plasmonic modulator. (b) Calculated conversion efficiency into SPPs initiated by tapering down a silicon waveguide, with the gap width and the Si taper length as parameters. (c) Schematic plan view of the second part of a coupling region between Si and plasmon waveguides in a whole plasmonic modulator. (d) Calculated coupling loss between the input Si waveguide and the plasmonic MZ waveguide, with the separation length and the Au taper length as parameters.

The abovementioned result has led to the conclusion that the total off-state insertion loss of the partial plasmonic modulator was 13.7 dB(8.1 dB + 2.8 dB × 2) with a total device length of 19.3 μm(6.5 μm + 6.4 μm × 2).

B. Whole Plasmonic Modulator

In the whole plasmonic modulator, an efficient mode conversion between an input light and the SPP mode can be realized by introducing tapered Si waveguides and *Y*-branch tapered metal slots at the front of the MIM MZ arms. To analyze the coupling efficiency, we divided the simulation area into the following two parts:

(A) An area from the Si waveguide to the MIM waveguide, i.e., the first half of the coupling region [see Fig. 6(a)].
(B) An area from the MIM waveguide to the MIM MZ arms equally divided by the *Y*-branch tapered metal slots, i.e., the second half of the coupling region [see Fig. 6(b)].

First, we calculated the conversion efficiency of the SPPs initiated by tapering down a Si waveguide. In the simulation,

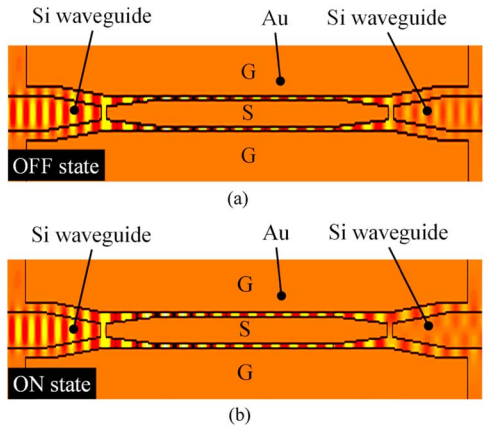

Fig. 7. Calculated mode field distribution of the whole plasmonic modulator embedded by the FTC. (a) on-state mode field distribution. A voltage of $+/-V_{\pi/2}$ is applied on the Au Island. (b) off-state mode field distribution.

Table 1. Comparison of Plasmon Modulators in Main Academic Institutions

Device	Main Research Group	$V_\pi L$ (V · mm)	Propagation Loss of MZ Arm	Total Insertion Loss	Size	Driving Voltage	Dimensions (nm) (W_{slot},h_{Au},h_{Si})	Ref.
Plasmon converter	KTH	–	–	5.5 dB/coupler	~3 pm/coupler	–	(100-200, 200, 250)	[35]
Plasmon converter	NTT	–	–	1.7 dB/coupler	~300 pm/coupler	–	(50, 20, 200)	[36]
Partial plasmonic mod. (w/M3)	KIT	1.3	~0.3 (dB/μm)	12 (dB)	34 (μm)[a]	7.5 (V)	(140, 150, 220)	[28]
Partial plasmonic mod. (w/YLD124/PSLD41)	KIT	0.45	0.4 (dB/μm)	27-34 (dB) (PS: 13-20, GC: 14)	29 (μm)[a]	5 (V)	(150, 150, 220)	[27]
Whole plasmonic mod. (w/DLD164)	ETH	0.06	0.5 (dB/μm)	37 (dB) (PS: 8, GC: 29)	10 (μm)[b]	1.5 (V)	(100, 220, 200)	[29,31]
Partial plasmonic IQ mod. (w/DLD164)	ETH	0.06	0.9 (dB/μm)	28.6 (dB) (PS: 12.6, GC: 16)	14 (μm)[a]	3 (V)	(100, 150, 220)	[32]
Partial plasmonic mod. (w/DLD164)	ETH	0.085	0.5 (dB/μm)	38.5 (dB) (PS: 12.5, GC: 26)	25 (μm)[a]	3.4 (V)	(80, 200, 220)	[30,31]
Partial plasmonic mod. (w/FTC-EO polymer)	Tokyo Tech	0.13	1.2 (dB/μm)	13.7 (dB) (PS: 13.7)	19.3 (μm)[a]	20 (V)	(50, 220, 220)	[this work]
Whole plasmonic mod. (w/FTC-EO polymer)	Tokyo Tech	0.13	1.2 (dB/μm)	15 (dB) (PS: 15)	21 (μm)[b]	20 (V)	(50, 220, 220)	[this work]

[a]MZ arm region.
[b]Whole device, PS, phase shifter; GC, grating coupler.

the dimension parameters are the same as those used in the analysis of the partial plasmonic modulators: taper length $L_{\text{Si-taper}}$ and gap width $W_{\text{Au-Si}}$. Figure 6(c) shows the calculated power ratio at the end point of the Si waveguide [denoted as the monitor line in Fig. 6(a)]. The trends shown in Fig. 6(c) are consistent with the results of the previous simulation for the partial plasmonic modulators. As a result, a maximum transmission ratio of 96% was obtained with 5.0-μm $L_{\text{Si-taper}}$ and 150-nm $W_{\text{Au-Si}}$.

Using these parameters, we finally calculated the coupling efficiency between the input Si waveguide and the entrance of the MIM MZ waveguide with metal-taper length $L_{\text{Au-taper}}$ and separation length L_{sep} as parameters (see Fig. 4). Figure 6(d) shows the calculated transmission ratio at the entrance of the MIM MZ arm [denoted as the monitor line in Fig. 6(b)]. Here, we also chose a flat end of the gold taper same as the Si waveguide. Otherwise a steeper inclination angle would increase the metal-induced reflection loss during the coupling. A maximum coupling efficiency of 45% (or a minimum coupling loss of 3.45 dB) was obtained when $L_{\text{Au-taper}}$ and L_{sep} were 2.0 μm and 200 nm, respectively.

Figure 7 shows the electric field distribution of the designed whole plasmonic modulator with and without an applied voltage of 20 V. We can see that appropriate π phase shift between the two MZ arms can be achieved with the applied voltage, and the intensity of light from the two MZ arms would be canceled.

The abovementioned result has led to the conclusion that the total insertion loss of the whole plasmonic modulator was 15 dB(8.1 dB + 3.45 dB × 2) with a total device length of 21 μm(6.5 μm + 7.25 μm × 2).

C. Comparison of the Plasmon Modulators in Main Academic Institutions

Table 1 lists the comparison of the performance of our device with that of the plasmon modulators developed by other research institutions. Our device can achieve a π phase shift with a relatively small device size and a low insertion loss compared with the structures proposed by other research groups [28–30,33], which is brought about the specific metal-taper structure and the FTC-EO polymer with an extremely large EO coefficient.

5. SUMMARY

In this paper, we have presented the analysis of two types of plasmonic push–pull modulators (i.e., the partial and whole plasmonic modulators) consisting of MZ interferometers with MIM slot waveguides embedded by the FTC-EO polymer. A π phase shift with a relatively small device size and a low insertion loss was obtained in our design by taking advantage of the strong optical confinement of the GSPP waveguide, enhanced EO coefficient of the FTC-EO polymer, and introduction of both tapered Si waveguides and Y-branch tapered metal slots. As a result, the partial and whole plasmonic modulators with a slot width of 50 nm and a driving voltage of 20 V can be 19.3 and 21 um long, leading to the off-state insertion losses of 13.7 and 15 dB.

Funding. Core Research for Evolutional Science and Technology (CREST); Japan Society for the Promotion of Science (JSPS), KAKENHI (14J02327, 15H05763, 15J11774, 16H06082, 16J11581).

REFERENCES

1. L. A. Coldren, "High performance InP-based photonic ICs—a tutorial," J. Lightwave Technol. **29**, 554–570 (2011).
2. R. Nagarajan, M. Kato, D. Lambert, P. Evans, S. Corzine, V. Lal, J. Rahn, A. Nilsson, M. Fisher, M. Kuntz, J. Pleumeekers, A. Dentai, H. Tsai, D. Krause, H. Sun, K. Wu, M. Ziari, T. Butrie, M. Reffle, M. Mitchell, F. Kish, and D. Welch, "Terabit/s class InP photonic integrated circuits," Semicond. Sci. Technol. **27**, 094003 (2012).

3. M. J. R. Heck, H.-W. Chen, A. W. Fang, B. R. Koch, D. Liang, H. Park, M. Sysak, and J. E. Bowers, "Hybrid silicon photonics for optical interconnects," IEEE J. Sel. Top. Quantum Electron. **17**, 333–346 (2011).
4. J. K. Doylend and A. P. Knights, "The evolution of silicon photonics as an enabling technology for optical interconnection," Laser Photon. Rev. **6**, 504–525 (2012).
5. E. Ozbay, "Plasmonics: merging photonics and electronics at nanoscale dimensions," Science **311**, 189–193 (2006).
6. N. Kinsey, M. Ferrera, V. M. Shalaev, and A. Boltasseva, "Examining nanophotonics for integrated hybrid systems: a review of plasmonic interconnects and modulators using traditional and alternative materials," J. Opt. Soc. Am. B **32**, 121–142 (2015).
7. D. K. Gramotnev and S. I. Bozhevolnyi, "Plasmonics beyond the diffraction limit," Nat. Photonics **4**, 83–91 (2010).
8. J. Takahara, S. Yamagishi, H. Taki, A. Morimoto, and T. Kobayashi, "Guiding of a one-dimensional optical beam with nanometer diameter," Opt. Lett. **22**, 475–477 (1997).
9. P. Berini, "Plasmon-polariton modes guided by a metal film of finite width," Opt. Lett. **24**, 1011–1013 (1999).
10. M. T. Hill, "Status and prospects for metallic and plasmonic nanolasers," J. Opt. Soc. Am. B **27**, B36–B44 (2010).
11. R. M. Ma, R. F. Oulton, V. J. Sorger, G. Bartal, and X. Zhang, "Room-temperature sub-diffraction-limited plasmon laser by total internal reflection," Nat. Mater. **10**, 110–113 (2010).
12. K. Ding, Z. C. Liu, L. J. Yin, M. T. Hill, M. J. H. Marell, P. J. van Veldhoven, R. Nöetzel, and C. Z. Ning, "Room-temperature continuous wave lasing in deep-subwavelength metallic cavities under electrical injection," Phys. Rev. B **85**, 041301 (2012).
13. M. Khajavikhan, A. Simic, M. Katz, J. H. Lee, B. Slutsky, A. Mizrahi, V. Lomakin, and Y. Fainman, "Thresholdless nanoscale coaxial lasers," Nature **482**, 204–207 (2012).
14. L. Liu, Z. Han, and S. He, "Novel surface plasmon waveguide for high integration," Opt. Express **13**, 6645–6650 (2005).
15. S. Zhu, T. Y. Liow, G. Q. Lo, and D. L. Kwong, "Silicon-based horizontal nanoplasmonic slot waveguides for on-chip integration," Opt. Express **19**, 8888–8902 (2011).
16. S. Zhu, G. Q. Lo, J. Xie, and D. L. Kwong, "Towards a thermal nanoplasmonic resonators based on Cu-TiO_2-Si hybrid plasmonic waveguide," in *Proceedings of Optical Fiber Communication (OFC)* (2013), paper OW3F.1.
17. M. W. Knight, H. Sobhani, P. Nordlander, and N. J. Halas, "Photodetection with active optical antennas," Science **332**, 702–704 (2011).
18. J. Fujikata, K. Nose, J. Ushida, K. Nishi, M. Kinoshita, T. Shimizu, T. Ueno, D. Okamoto, A. Gomyo, M. Mizuno, T. Tsuchizawa, T. Watanabe, K. Yamada, S. Itabashi, and K. Ohashi, "Waveguide-integrated Si nano-photodiode with surface-plasmon antenna and its application to on-chip optical clock distribution," Appl. Phys. Express **1**, 022001 (2008).
19. I. Goykhman, B. Desiatov, J. Khurgin, J. Shappir, and U. Levy, "On chip plasmonic enhanced silicon Schottky detector for telecom wavelengths," in *Proceedings of Optical Fiber Communication (OFC)* (2012), paper OTu2D.3.
20. S. Muehlbrandt, A. Melikyan, T. Harter, K. Köhnle, A. Muslija, P. Vincze, S. Wolf, P. Jakobs, Y. Fedoryshyn, W. Freude, J. Leuthold, C. Koos, and M. Kohl, "Silicon-plasmonic internal-photoemission detector for 40 Gbit/s data reception," Optica **3**, 741–747 (2016).
21. Y. Enami, P. Poyhonen, and D. Mathine, "Poling of soda-lime glass for hybrid glass/polymer electro-optic modulators," Appl. Phys. Lett. **76**, 1086–1088 (2000).
22. R. A. Pala, K. T. Shimizu, N. A. Melosh, and M. L. Brongersma, "A nonvolatile plasmonic switch employing photochromic molecules," Nano Lett. **8**, 1506–1510 (2008).
23. T. Amemiya, E. Murai, Z. Gu, N. Nishiyama, and S. Arai, "GaInAsP/InP-based optical modulator consisting of gap-surface-plasmon-polariton waveguide: theoretical analysis," J. Opt. Soc. Am. B **31**, 2908–2913 (2014).
24. K. F. MacDonald, Z. L. Sámson, M. I. Stockman, and N. I. Zheludev, "Ultrafast active plasmonics," Nat. Photonics **3**, 55–58 (2008).
25. S. Zhu, G. Lo, and D.-L. Kwong, "Ultracompact Si electro-optic modulator based on horizontal Cu-insulator-Si-insulator-Cu nanoplasmonic waveguide," in *Proceedings of Optical Fiber Communication (OFC)* (2013), paper OTh1D.5.
26. W. Cai, J. S. White, and M. L. Brongersma, "Power-efficient electro-optic plasmonic modulators," Nano Lett. **9**, 4403–4411 (2009).
27. A. Melikyan, K. Koehnle, M. Lauermann, R. Palmer, S. Koeber, S. Muehlbrandt, P. C. Schindler, D. L. Elder, S. Wolf, W. Heni, C. Haffner, Y. Fedoryshyn, D. Hillerkuss, M. Sommer, L. R. Dalton, D. Van Thourhout, W. Freude, M. Kohl, J. Leuthold, and C. Koos, "Plasmonic-organic hybrid (POH) modulators for OOK and BPSK signaling at 40 Gbit/s," Opt. Express **23**, 9938–9946 (2015).
28. A. Melikyan, L. Alloatti, A. Muslija, D. Hillerkuss, P. C. Schindler, J. Li, R. Palmer, D. Korn, S. Muehlbrandt, D. Van Thourhout, B. Chen, R. Dinu, M. Sommer, C. Koos, M. Kohl, W. Freude, and J. Leuthold, "High-speed plasmonic phase modulators," Nat. Photonics **8**, 229–233 (2014).
29. C. Haffner, W. Heni, Y. Fedoryshyn, J. Niegemann, A. Melikyan, D. L. Elder, B. Baeuerle, Y. Salamin, A. Josten, U. Koch, C. Hoessbacher, F. Ducry, L. Juchli, A. Emboras, D. Hillerkuss, M. Kohl, L. R. Dalton, C. Hafner, and J. Leuthold, "All-plasmonic Mach–Zehnder modulator enabling optical high-speed communication at the microscale," Nat. Photonics **9**, 525–528 (2015).
30. W. Heni, C. Haffner, B. Baeuerle, Y. Fedoryshyn, A. Josten, D. Hillerkuss, J. Niegemann, A. Melikyan, M. Kohl, D. L. Elder, L. R. Dalton, C. Hafner, and J. Leuthold, "108 Gbit/s plasmonic Mach–Zehnder modulator with >70-GHz electrical bandwidth," J. Lightwave Technol. **34**, 393–400 (2016).
31. C. Haffner, W. Heni, Y. Fedoryshyn, J. Arne, B. Baeuerle, C. Hoessbacher, Y. Salamin, U. Koch, U. Dordevic, P. Mousel, R. Bonjour, A. Emboras, D. Hillerkuss, P. Leuchtmann, D. L. Elder, L. Dalton, C. Hafner, and J. Leuthold, "Plasmonic organic hybrid modulators—scaling highest speed photonics to the microscale," Proc. IEEE **104**, 2362–2379 (2016).
32. W. Heni, C. Hoessbacher, C. Haffner, Y. Fedoryshyn, B. Baeuerle, A. Josten, D. Hillerkuss, Y. Salamin, R. Bonjour, A. Melikyan, M. Kohl, D. L. Elder, L. R. Dalton, C. Hafner, and J. Leuthold, "High speed plasmonic modulator array enabling dense optical interconnect solutions," Opt. Express **23**, 29746–29757 (2015).
33. C. Hoessbacher, Y. Salamin, Y. Fedoryshyn, W. Heni, A. Josten, B. Baeuerle, C. Haffner, M. Zahner, H. Chen, D. L. Elder, S. Wehrli, D. Hillerkuss, D. Van Thourhout, J. Van Campenhout, L. R. Dalton, C. Hafner, and J. Leuthold, "Optical interconnect with densely integrated plasmonic modulator and germanium photodetector arrays," in *Proceedings of Optical Fiber Communication (OFC)* (2016), paper Th1F.6.
34. S. Zhu, G. Q. Lo, and D. L. Kwong, "Theoretical investigation of silicon MOS-type plasmonic slot waveguide based MZI modulators," Opt. Express **18**, 27802–27819 (2010).
35. J. Tian, S. Yu, W. Yan, and M. Qiu, "Broadband high-efficiency surface-plasmon-polariton coupler with silicon-metal interface," Appl. Phys. Lett. **95**, 013504 (2009).
36. M. Ono, H. Taniyama, H. Xu, M. Tsunekawa, E. Kuramochi, K. Nozaki, and M. Notomi, "Deep-subwavelength plasmonic mode converter with large size reduction for Si-wire waveguide," Optica **3**, 999–1005 (2016).
37. T. Yamada, I. Aoki, H. Miki, C. Yamada, and A. Otomo, "Effect of methoxy or benzyloxy groups bound to an amino-benzene donor unit for various nonlinear optical chromophores as studied by hyper-Rayleigh scattering," Mater. Chem. Phys. **139**, 699–705 (2013).
38. T. Yamada and A. Otomo, "Usefulness of transmission ellipsometric method for evaluation of electro-optic materials," IEICE Trans. Electron. **E98**-C, 143–146 (2015).